Numerical solution of the Transient Free Convection in Magneto-Micropolar Fluid past vertical semi-infinite porous plate with Heat Generation, Mass Transfer and Constant Heat Flux subjected to Magnetic Field

N.M. Mutua, M. N. Kinyanjui, J.K. Kwanza, F.K. Gatheri

Abstract— Numerical solution of the Transient Free Convection in Magneto-Micropolar Fluid past vertical semi-infinite porous plate with Heat Generation, Mass Transfer and Constant Heat Flux subjected to Magnetic Field is studied. The plate considered is porous and the Micropolar incompressible fluid that is electrically conducting flows past the semi-infinite vertical inclined plate subjected to variable inclined magnetic field. Fluid is injected through the plate at a constant velocity. The general solution of the coupled governing non-linear partial equations is obtained from the equation of linear momentum, angular momentum, energy equation and concentration equation, which is valid for every value of time t. The Trivariate Spectral Collocation Method (TSCM) and a MATLAB computer program are employed in solving the arising non-linear partial differential equations in order to generate the velocity, angular momentum, temperature and concentration profiles. The effects of the various parameters entering into the flow problem are presented graphically and discussed. These parameters include the Magnetic parameter, the Schmidt number, the Micropolar parameter, the suction parameter, the Eckert number, the Soret number, the Prandtl number, the Grashof number, the heat source parameter, Dimensionless material parameter and Micro-rotation parameter. The values proportional to coefficient of Skin friction, Nusselt number and Sherwood number are also computed numerically, tabulated and discussed. The effect of changing the parameters mentioned above is observed either to increase, to decrease or to have no effect on the velocity profiles, the angular momentum profiles, the temperature profiles, the concentration profiles, the skin friction and the rates of heat and mass transfer.

Index Terms— Heat Flux, Magnetohydrodynamics, Magnetic Field, Micropolar Fluid, Prorous, Semi-infinite, Trivariate Spectral Collocation.

1 INTRODUCTION

THE equations governing hydrodynamics flows are highly non-linear PDEs thus not possible to obtain analytical solutions. In this chapter, mathematical analysis of the study is given, governing equations are stated and non-dimensionalised, Trivariate Spectral Collocation Method and a MATLAB algorithm are employed in solving the PDEs. Finally, investigations are carried out on how the variation of the various parameters affect the linear velocity, angular velocity, temperature and concentration profiles. The rate of heat and mass transfer are also computed by applying the Nusselt number and the Sherwood number.

Magnetohydrodynamic (MHD) convection micropolar flow has many important engineering applications in cooling hot material like steel plates at ROT [1], in cooling of combustion engines and electronic microchips [2], in setting up the ink-jet printers [3,4], in evaporation of refrigerant-oil mixture [5], in Erosion threshold of a liquid immersed granular bed [6], analysing blood flow [7,24], polymeric suspensions [8], lab-on-a chip [9,25] rigid-rod epoxies [10].

The micropolar theory shows micro-rotation effects as well as micro inertia contributions has many applications such as polymer fluids, liquid crystals, animal bloods, unusual lubricants, colloidal and suspension solutions, colloidal fluids, liquid crystals, and polymeric suspension.

[11] investigated micropolar fluid over a stretching surface in a non-Darcian porous medium when viscosity and thermal conductivity vary with temperature in presence of magnetic field. [12] was the first to formulate the theory of micro polar fluids. In essence, the theory introduces new material parameters, an additional independent vector field, the micro rotation and new constitutive equations, which must be solved simultaneously with the usual equations for Newtonian flow. The desire to model the non-Newtonian flow of fluid containing rotating micro-constituents provided initial motivation for the development of the theory, but subsequent studies have successfully applied the model to a wide range of applications including blood flow, lubricants, porous media, turbulent shear flows and flowing capillaries and micro channels [13].

[14] analysed Melting Heat Transfer and Induced-Magnetic Field Effects on the Micropolar Fluid Flow towards Stagnation Point using Boundary Layer Analysis. Their results indicated that due to the formation of boundary layer on melting surface (region of low heat energy) in the presence of induced magnetic field, space and temperature dependent internal heat generation enhances the heat transfer rate. [26] explored the Chemical reaction and thermal radiation effects on MHD micropolar fluid past a stretching sheet embedded in a non-Darcian porous medium. It was established that the increase in Schmidt number and chemical reaction caused a decrease in the skin-friction coefficient and an increase in the mass transfer rate.

[16] studied Similarity Solution of Unsteady Boundary Layer Flow of Nanofluids past a Vertical Plate with Convective Heating. It was inferred that the velocity and temperature of nanofluid decreases as a result of increasing unsteadiness parameter while the velocity and the temperature distributions decrease by decreasing Biot number. Effects of Variable Viscosity and Thermal Conductivity of Unsteady Micropolar Fluid under Mixed Convection in Presence of Uniform Magnetic Field on Stretching Surface was studied by [17]. In their study it was observed that within the boundary layer thermal conductivity and viscosity parameter along with other parameters have a significant effect on velocity, micro-rotation, temperature distribution and magnetic field.

[18] researched on MHD and radiation effects on mixed convection unsteady flow of micropolar fluid over a stretching sheet. They found out that there is a smooth transition from small-time solution to the large-time solution. The Numerical study of MHD micropolar Carreau nanofluid in the presence of induced magnetic field was carried out by [19]. It was noted that the dimensionless velocity is enhanced for the Weissenberg number and the power law index while reverse situation is studied in the thermal and the concentration profile.

[20] investigated Soret and Dufour Effects on Steady free Convection in MHD Micropolar Fluid Flow, Mass and Heat Transfer with Hall Current. It was observed that the temperature profile increases as Pr and Df increases

2 MODEL DESCRIPTION

2.1 Mathematical Formulation

Consider the Stokes problem of free convection unsteady flow of a viscous incompressible electrically conducting micropolar fluid between along the semi-infinite (unbounded in one direction or dimension) porous vertical plate in presence of a transverse magnetic field **B** applied parallel to y-axis which is normal to the plate. The temperature of the plate is held at constant value of T_s and the heat flux is considered as constant, the thermal dispersion effect is also included. We have considered z-axis along the plate in the vertical direction and y-axis perpendicular to the plate. The flow configuration of the semi-infinite plate and the two-dimensional Cartesian coordinate system are shown in figure 1.

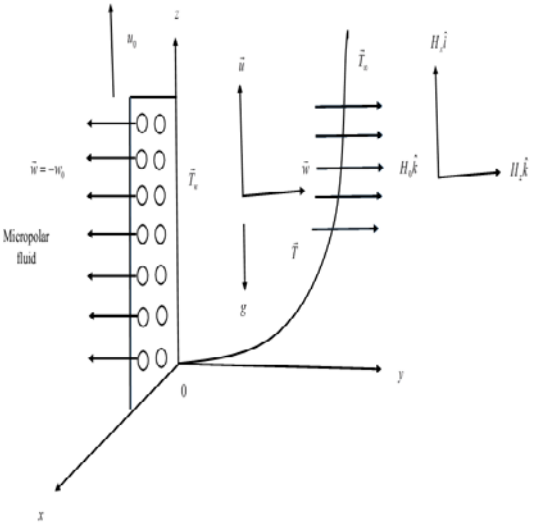

Fig. 1. Physical Model and Coordinate system

The plate is semi-infinite along y and z-axis directions and is non-conducting, thus all physical quantities will be functions of *y, z* and *t* only. Injection of the fluid takes place through the porous walls of the plate with uniform velocity W_0, which is greater than zero for injection and less than zero for suction. It is assumed that no applied or polarization voltages exist since the plate is insulated. This corresponds to the case where no energy is being added or extracted from the fluid by electrical means. (i.e. electric field $E = 0$).

In general, the electric current flowing in the fluid gives rise to an induced magnetic field which perturbs the applied magnetic field. Since magnetic Reynolds number is very small for metallic liquids and partially ionized fluids so the induced magnetic field may be neglected in comparison to the applied one.

Under the above assumptions, the governing equations of the flow with the Boussinesq's approximation can be put in the following form;

Mass Conservation Equation

$$\frac{\partial u}{\partial x}+\frac{\partial w}{\partial z}=0\,. \tag{1}$$

Linear Momentum Conservation Equation

$$\frac{\partial u}{\partial t}+u\frac{\partial u}{\partial x}+w\frac{\partial u}{\partial z}=\left(\frac{\mu+k}{\rho}\right)\frac{\partial^2 u}{\partial z^2}+\left(\frac{k}{\rho}\right)\frac{\partial N}{\partial z}+g*\beta\left(T-T_\infty\right)+g*\beta'\left(C-C_\infty\right) -\frac{\sigma B_0^2 U}{\rho}-\frac{\upsilon u}{\rho K_p^*} \tag{2}$$

Equation of conservation of Angular Momentum

$$\rho j\left(\frac{\partial N}{\partial t}+u\frac{\partial N}{\partial x}+w\frac{\partial N}{\partial z}\right)=\gamma\frac{\partial^2 N}{\partial z^2}-k\left(2N+\frac{\partial u}{\partial t}\right) \tag{3}$$

Equation of Energy

$$\frac{\partial T}{\partial t}+u\frac{\partial T}{\partial x}+w\frac{\partial T}{\partial z}=\frac{k'}{\rho j}\frac{\partial^2 T}{\partial z^2}+Q\left(T-T_\infty\right) \tag{4}$$

Species Concentration Equation

$$\frac{\partial C}{\partial t}+u\frac{\partial C}{\partial x}+w\frac{\partial C}{\partial z}=D'\frac{\partial^2 C}{\partial z^2} \tag{5}$$

Subject to the Boundary Conditions:

$$\left.\begin{aligned} &u(x,0,t)=0,\ \ N(x,0,t)=0,\ T(x,0,t)=T_s,\ C(x,0,t)=C_s \\ &u(x,\infty,t)=0,\ \ N(x,\infty,t)=0,\ T(x,\infty,t)=T_\infty,\ C(x,\infty,t)=C_\infty \end{aligned}\right\} \tag{6}$$

2.2 Non-dimesionalisation

Nondimensionalization is the process of removal of units from physical quantities by a suitable substitution of variables. A non-dimensionalised equation is one in which each term in the equation is dimensionless. Dynamic similarity requires that the ratio of all forces be the same. The ratio of different forces produces many of the key non-dimensional parameters in fluid mechanics. These groups occur regularly when dimensional analysis is applied to fluid-dynamical problems. They can be derived by considering forces on a small volume of fluid. They can also be derived by non-dimensionalizing the differential equations of fluid flow.

Making the values dimensionless using the following substitution:

$$\left.\begin{aligned} &u^*=\frac{u}{U_0},\ w^*=\frac{w}{W_0},\ x^*=\frac{U_0}{\nu}x,\ w^*=\frac{U_0}{\nu}w,\ t^*=\frac{U_0^2}{\nu}t, \\ &N^*=\frac{\nu}{U_0^2}N,\ j^*=\frac{U_0^2}{\nu^2}j,\ \theta=\frac{(T-T_\infty)}{(T_s-T_\infty)},\ \phi=\frac{(C-C_\infty)}{(C_s-C_\infty)} \end{aligned}\right\} \tag{7}$$

Introducing the following non-dimensionless quantities which are of engineering interest;

Prandtl Number, $\Pr=\dfrac{\nu}{k/\rho C_p}=\dfrac{\nu\rho C_p}{k}$, Grashof Number, $Gr=\dfrac{\nu g*\beta\left(T_s-T_\infty\right)}{U_0^3}$, Modified Grashof Number, $Gc=\dfrac{g*\beta c\nu\left(C_s-C_\infty\right)}{U_0^3}$

$\lambda=\dfrac{\gamma}{\rho\nu j}$, $\Delta=\dfrac{k}{\rho\upsilon}=\dfrac{k}{\mu}$ Dimensionless material parameters

Here u and w are velocity components associated with x and z directions measured along and normal to the vertical plate respectively, ν the kinematic coefficient of viscosity, k the vortex viscosity, ρ the density of the fluid, $g*$ the acceleration due to gravity, β the coefficient of thermal expansion, T the temperature of the fluid in the boundary layer, T_∞ the free steam temperature, N the angular velocity, γ the spin gradient viscosity, j the microinertia per unit mass, k' the thermal conductivity, C_p specific heat at constant pressure and Q the heat generation.

Non-dimensionalizing equations (2) -(5) yields the final set of equations as;

$$\frac{\partial u}{\partial x}+\frac{\partial w}{\partial z}=0 \tag{8}$$

$$\frac{\partial u}{\partial t}+u\frac{\partial u}{\partial x}-S\frac{\partial u}{\partial z}=(1+\Delta)\frac{\partial^2 u}{\partial z^2}+Gr\theta+Gc\phi+\Delta\frac{\partial N}{\partial z}-\left(M+\frac{1}{K}\right)u \tag{9}$$

$$\frac{\partial N}{\partial t}+u\frac{\partial N}{\partial x}-S\frac{\partial N}{\partial z}=\lambda\frac{\partial^2 N}{\partial z^2}-\frac{\Delta}{j}\left(2N+\frac{\partial u}{\partial z}\right) \tag{10}$$

$$\frac{\partial \theta}{\partial t}+u\frac{\partial \theta}{\partial x}-S\frac{\partial \theta}{\partial z}=\frac{1}{\Pr}\frac{\partial^2 \theta}{\partial z^2}+\alpha\theta+Ec(1+\Delta)\left(\frac{\partial u}{\partial z}\right)^2 \tag{11}$$

$$\frac{\partial \phi}{\partial t}+u\frac{\partial \phi}{\partial x}-S\frac{\partial \phi}{\partial z}=\frac{1}{Sc}\frac{\partial^2 \phi}{\partial z^2} \tag{12}$$

The boundary conditions are transformed as;

$$\begin{aligned}&u(x,0,t)=0,\ N(x,0,t)=0,\ \theta(x,0,t)=1,\ \phi(x,0,t)=1\\&u(x,\infty,t)=0,\ N(x,\infty,t)=0,\ \theta(x,\infty,t)=1,\ \phi(x,\infty,t)=1\end{aligned} \tag{13}$$

3 Trivariate Spectral Collocation Method of solution for two dimensional Partial Differential Equations arising in fluid mechanics

As demonstrated in this document, the numbering for sections upper case Arabic numerals, then upper case Arabic numerals, separated by periods. Initial paragraphs after the section title are not indented. Only the initial, introductory paragraph has a drop cap.

In this section, we describe the algorithm for solving a system of two-dimensional partial differential equations that defines the problem of the transient free convection in magneto micropolar fluid with heat generation, mass transfer and constant heat flux. The present investigation on the numerical method involves application of a purely spectral collocation discretization is applied on space and time variables. The system of PDEs considered takes the form;

$$\frac{\partial u}{\partial t}+u\frac{\partial u}{\partial x}-S\frac{\partial u}{\partial z}=(1+\Delta)\frac{\partial^2 u}{\partial z^2}+Gr\theta+Gc\phi+\Delta\frac{\partial N}{\partial z}-\left(M+\frac{1}{K}\right)u \tag{14}$$

$$\frac{\partial N}{\partial t}+u\frac{\partial N}{\partial x}-S\frac{\partial N}{\partial z}=\lambda\frac{\partial^2 N}{\partial z^2}-\frac{\Delta}{j}\left(2N+\frac{\partial u}{\partial z}\right) \tag{15}$$

$$\frac{\partial \theta}{\partial t}+u\frac{\partial \theta}{\partial x}-S\frac{\partial \theta}{\partial z}=\frac{1}{\Pr}\frac{\partial^2 \theta}{\partial z^2}+\alpha\theta+Ec(1+\Delta)\left(\frac{\partial u}{\partial z}\right)^2 \tag{16}$$

$$\frac{\partial \phi}{\partial t}+u\frac{\partial \phi}{\partial x}-S\frac{\partial \phi}{\partial z}=\frac{1}{Sc}\frac{\partial^2 \phi}{\partial z^2} \tag{17}$$

Eqs.3.16-3.19 are solved subject to boundary conditions

$$\begin{aligned}&u(x,0,t)=0,\ N(x,0,t)=0,\ \theta(x,0,t)=1,\ \phi(x,0,t)=1\\&u(x,\infty,t)=0,\ N(x,\infty,t)=0,\ \theta(x,\infty,t)=1,\ \phi(x,\infty,t)=1\end{aligned} \tag{18}$$

and the initial conditions

$$u(x,y,0)=0,\ N(x,y,0)=0,\ \theta(x,y,0)=0,\ \phi(x,y,0)=0 \tag{19}$$

In view of the non-linearity in Eq.16 and the coupling of the partial differential equations Eqs.14-18, we simplify the differential equations using relaxation method. In the relaxation method, it is assumed that all nonlinear terms are known from the previous iteration while at the same time decoupling the system of differential equations using the Gauss-Seidel approach. Applying the relation method, we obtained the decoupled system of equations;

$$(1+\Delta)\frac{\partial^2 u_{s+1}}{\partial z^2}+S\frac{\partial u_{s+1}}{\partial z}-\left(M+\frac{1}{K}\right)u_{s+1}-\frac{\partial u_{s+1}}{\partial t}=-u_s\frac{\partial u_s}{\partial x}-Gr\theta_s-Gc\phi_s-\Delta\frac{\partial N_s}{\partial z} \tag{20}$$

$$\lambda\frac{\partial^2 N_{s+1}}{\partial z^2}+S\frac{\partial N_{s+1}}{\partial z}-u_{s+1}\frac{\partial N_{s+1}}{\partial x}+\frac{2\Delta}{j}N_{s+1}-\frac{\partial N_{s+1}}{\partial t}=-\frac{\Delta}{j}\frac{\partial u_{s+1}}{\partial z} \tag{21}$$

$$\frac{1}{\Pr}\frac{\partial^2 \theta_{s+1}}{\partial z^2}+S\frac{\partial \theta_{s+1}}{\partial z}-u_{s+1}\frac{\partial \theta_{s+1}}{\partial x}-\frac{\partial \theta_{s+1}}{\partial t}-\alpha\theta_{s+1}=-Ec(1+\Delta)\left(\frac{\partial u_{s+1}}{\partial z}\right)^2 \tag{22}$$

$$\frac{1}{Sc}\frac{\partial^2 \phi_{s+1}}{\partial z^2}+S\frac{\partial \phi_{s+1}}{\partial z}-u_{s+1}\frac{\partial \phi_{s+1}}{\partial x}-\frac{\partial \phi_{s+1}}{\partial t}=0 \tag{23}$$

where small s signifies the previous iteration level. Using initial approximations to solutions of the partial differential equations as u_0, N_0, θ_0, and ϕ_0, the Gauss-Seidel relaxation scheme Eqs.(20)-(23) is solved iteratively until the solution converges. As a rule of thumb, a simple choice of the initial approximation to the solution is a polynomial that satisfies the given boundary conditions. The semi-infinite domain of approximation $[0,\infty)$ is truncated into a finite domain $[0,L]$ where L is taken to be large enough to approximate conditions at infinity. The finite domain of approximation is discretized into Chebyshev Gauss-Lobatto nodes defined in Eq. (3.61) as

$$\begin{aligned}&\{\hat{x}_i\}_{i=0}^{N_x}=\cos\left(\frac{i\pi}{N_x}\right),\ \hat{x}(x)=\frac{2}{b-a}\left[x-\frac{1}{2}(b+a)\right],\ x\in[a,b],\\&\{\hat{z}_j\}_{j=0}^{N_z}=\cos\left(\frac{j\pi}{N_z}\right),\ \hat{z}(z)=\frac{2}{L}\left[z-\frac{L}{2}\right],\ z\in[0,L],\\&\{\hat{t}_k\}_{k=0}^{N_t}=\cos\left(\frac{k\pi}{N_t}\right),\ \hat{t}(t)=\frac{2}{T}\left[t-\frac{T}{2}\right],\ t\in[0,T]\end{aligned} \tag{24}$$

Here $[a,b]$ is the interval of approximation in the x-direction and T is the final time. The objects N_x, N_z, N_t are the grid points in x, z, and t, respectively. In the solution process, the approximate solution of the PDEs Eqs. (14)-(18) is assumed to be the Trivariate Lagrange interpolating polynomials. For illustrative purposes, we shall consider the solution to the unknown function $u(x,z,t)$ that takes the form;

$$u(x,z,t)\approx U(x,z,t)=\sum_{p=0}^{N_x}\sum_{q=0}^{N_z}\sum_{r=0}^{N_t}U(x_p,z_q,t_r)L_p(x)L_q(z)L_r(t) \tag{25}$$

- N.M.Mutua, Taita Taveta University, Department of Mathematics, Statistics & Physical Sciences, Kenya, P.O.Box, 635-80300, nicholasmutha-ma@ttu.ac.ke
- M.N.Kinyanjui, JKUAT, Department of Pure & Applied Mathematics, Kenya, P.O.Box, 62000-00200, mathewkiny@jkuat.ac.ke
- J.K.Kwanza, JKUAT, Department of Pure & Applied Mathematics, Kenya, P.O.Box, 62000-00200, jKwanza@jkuat.ac.ke
- F.K.Gatheri, Technical University of Kenya, School of Mathematics and Statistics, Kenya, P.O.Box 52428-00200, kgatheri@yahoo.com

The spatial differentiation matrix in x is approximated at the collocation nodes $(\hat{x}_i, \hat{y}_j, t_k)$, for $j = 0,1,2,\ldots\ldots, N_z$, and $k = 0,1,2,\ldots\ldots, N_t$, as follows;

$$\frac{\partial u}{\partial t}(\hat{x}_i, \hat{z}_j, \hat{t}_k) \approx \sum_{p=0}^{N_x}\sum_{q=0}^{N_z}\sum_{r=0}^{N_t} U(x_p, z_q, t_r) L'_p(\hat{x}_i) L_q(\hat{z}_j) L_r(\hat{t}_k) = \sum_{p=0}^{N_x} U(x_p, z_q, t_k) L'_p(\hat{x}_i) = D\bigcup_k^j = \left(\frac{2}{b-a}\right) D\bigcup_k^j \quad (26)$$

Where $\hat{D} = \left(\frac{b-a}{2}\right)D$ is the standard first order Chebyshev differentiation matrix of size $(N_x+1)\times(N_x+1)$ as defined by [Magagula, 2016]. The higher order differentiation matrices are obtained using matrix multiplication. The vector $\bigcup_k^j$ is defined as

$$\bigcup_k^j = \left[u(x_0, z_j, t_k), u(x_1, z_j, t_k), \ldots\ldots\ldots\ldots, u(x_{N_x}, z_j, t_k)\right], \quad j = 0,1,\ldots., N_z,\ k = 0,1,\ldots., N_t \quad (27)$$

where T denotes matrix transpose. Similarly, the spatial differentiation matrix in **y** is approximated at the collocation points $(\hat{x}_i, \hat{z}_j, \hat{t}_k)$, for $i = 0,1,2\ldots, N_x$ and $k = 0,1,2,\ldots, N_t$ as

$$\frac{\partial u}{\partial z}(\hat{x}_i, \hat{y}_j, \hat{t}_k) \approx \sum_{q=0}^{N_z} U(x_i, y_q, t_k) L'_q(\hat{z}_j) = \sum_{q=0}^{N_z} D_{j,q}\bigcup_k^q = \sum_{q=0}^{N_z}\left(\frac{2}{L}\right)\hat{D}_{j,q}\bigcup_k^q \quad (28)$$

Where $\hat{\hat{D}} = \left(\frac{L}{2}\right)\overline{D}_{j,q}$, $j,q = 0,1,2,\ldots\ldots, N_z$, are entries of a standard first order Chebyshev differentiation matrix of size $(N_z+1)\times(N_z+1)$. Higher order differentiation matrix with respect to z can be obtained using matrix multiplication. Finally, we approximate the differentiation matrix in t at the collocation points $(\hat{x}_i, \hat{z}_j, \hat{t}_k)$, for $i = 0,1,2\ldots, N_x$, and $j = 0,1,2,\ldots, N_z$, as;

$$\frac{\partial u}{\partial t}(\hat{x}_i, \hat{z}_j, \hat{t}_k) \approx \sum_{r=0}^{N_t}\sum_{q=0}^{N_z} U(x_i, y_j, t_r) L'_r(\hat{t}_k) = \sum_{q=0}^{N_z} D_{j,q}\bigcup_k^q = \sum_{r=0}^{N_t}\sum_{q=0}^{N_z}\overline{\overline{D}}_{k,r}\bigcup_r^q \quad (29)$$

Where $\hat{\hat{D}}_{k,r} = \left(\frac{T}{2}\right)\overline{\overline{D}}_{k,r}$, $k,r = 0,1,2,\ldots\ldots, N_t$, are entries of a standard first order Chebyshev differentiation matrix of size $(N_t+1)\times(N_t+1)$. We remark that the bar in $\overline{D}$ at Eq. (28) and double bar in $\overline{\overline{D}}$ at Eq. (29) distinguishes the differentiation matrix in z and t, respectively, from that in x. We note that in generating the sequence of vectors $\bigcup_k^j$, $j = 0,1,2,\ldots\ldots, N_z$, $k = 0,1,2,\ldots\ldots, N_t$, the superscript j is varied of each subscript k. Such a pattern will be useful when assembling the system of linear algebraic equations to obtain coefficient matrices. The partial derivatives of the unknowns N, θ, ϕ are approximated in a similar manner.

Using Eq. (26), Eq. (28) and Eq. (29) in the scheme Eqs. (20)-(23), we obtain a $(N_t+1)\times(N_y+1)\times(N_x+1)$ decoupled system of linear algebraic equations given by;

$$\left(M+\frac{1}{K}\right)\bigcup_k^j + \sum_{q=0}^{N_z}\left[(1+\Delta)\overline{D}_{j,q}^2 + S\overline{D}_{j,q}\right]\bigcup_k^q - \sum_{r=0}^{N_t}\sum_{q=0}^{N_z}\overline{\overline{D}}_{k,r}\bigcup_r^q = R_1 \quad (30)$$

$$\left[-u_{s+1}D + \frac{2\Delta}{j}\mathrm{I}\right]\mathrm{N}_r^q + \sum_{q=0}^{N_z}\left[\lambda\overline{D}_{j,q}^2 + S\overline{D}_{j.q}\right]\mathrm{N}_k^q - \sum_{r=0}^{N_t}\sum_{q=0}^{N_z}\overline{\overline{D}}_{k,r}\mathrm{N}_r^q = R_2 \quad (31)$$

$$\left[-u_{s+1}D\right]\Theta_r^q + \sum_{q=0}^{N_z}\left[\frac{1}{\mathrm{Pr}}\overline{D}_{j,q}^2 + S\overline{D}_{j.q}\right]\Theta_k^q - \sum_{r=0}^{N_t}\sum_{q=0}^{N_z}\overline{\overline{D}}_{k,r}\Theta_r^q = R_3 \quad (32)$$

$$\left[-u_{s+1}D\right]\Phi_k^j + \sum_{q=0}^{N_z}\left[\frac{1}{Sc}\overline{D}_{j,q}^2 + S\overline{D}_{j.q}\right]\Phi_k^q - \sum_{r=0}^{N_t}\sum_{q=0}^{N_z}\overline{\overline{D}}_{k,r}\Phi_r^q = R_4 \quad (33)$$

where I is an identity matrix of size $(N_x+1)\times(N_x+1)$. The right-hand side of equations Eqs. (30)-(33) is defined as

$$\left.\begin{aligned} R_1 &= -u_s\frac{\partial u_s}{\partial x} - Gr\theta_s - Gc\phi_s - \Delta\frac{\partial \mathrm{N}_s}{\partial z},\ R_2 = -\frac{\Delta}{j}\frac{\partial u_{s+1}}{\partial z}, \\ R_3 &= -Ec(1+\Delta)\frac{\Delta}{j}\left(\frac{\partial u_{s+1}}{\partial z}\right)^2,\ R_4 = 0 \end{aligned}\right\} \quad (34)$$

where **0** is a zero vector of size $(N_t+1)\times(N_y+1)\times(N_x+1)\times 1$. The initial condition $u(x,z,t)$ when evaluated at the collocation points yields

$$u(x_i, z_j, 0) = u(x_i, y_j, t_{N_t}) = 0 = \bigcup_{N_t}^j \quad (35)$$

The initial conditions corresponding to the other unknowns are evaluated in a similar manner. The initial conditions reduce Eqs. (30)-(33) to

$$\left(M+\frac{1}{K}\right)\bigcup_k^j + \sum_{q=0}^{N_z}\left[(1+\Delta)\overline{D}_{j,q}^2 + S\overline{D}_{j,q}\right]\bigcup_k^q - \sum_{r=0}^{N_t-1}\sum_{q=0}^{N_z}\overline{\overline{D}}_{k,r}\bigcup_r^q = R_1 \quad (36)$$

$$\left[-u_{s+1}D + \frac{2\Delta}{j}\mathrm{I}\right]\mathrm{N}_k^j + \sum_{q=0}^{N_z}\left[\lambda\overline{D}_{j,q}^2 + S\overline{D}_{j.q}\right]\mathrm{N}_k^q - \sum_{r=0}^{N_t-1}\sum_{q=0}^{N_z}\overline{\overline{D}}_{k,r}\mathrm{N}_r^q = R_2 \quad (37)$$

$$\left[-u_{s+1}D\right]\Theta_k^j + \sum_{q=0}^{N_z}\left[\frac{1}{\mathrm{Pr}}\overline{D}_{j,q}^2 + S\overline{D}_{j.q}\right]\Theta_k^q - \sum_{r=0}^{N_t-1}\sum_{q=0}^{N_z}\overline{\overline{D}}_{k,r}\Theta_r^q = R_3 \quad (38)$$

$$\left[-u_{s+1}D\right]\Phi_k^j + \sum_{q=0}^{N_z}\left[\frac{1}{Sc}\overline{D}_{j,q}^2 + S\overline{D}_{j.q}\right]\Phi_k^q - \sum_{r=0}^{N_t-1}\sum_{q=0}^{N_z}\overline{\overline{D}}_{k,r}\Phi_r^q = R_4 \quad (39)$$

$$\left.\begin{aligned} &u_{s+1}(x, zN_z, t) = 0,\ N_{s+1}(x, zN_z, t) = 0,\ \theta_{s+1}(x, zN_z, t) = 1,\ \phi_{s+1}(x, zN_z, t) = 1 \\ &u_{s+1}(x, z_0, t) = 0,\ N_{s+1}(x, z_0, t) = 0,\ \theta_{s+1}(x, z_0, t) = 1,\ \phi_{s+1}(x, z_0, t) = 1 \end{aligned}\right\} \quad (40)$$

Eqs. (36)-(39) are solved subject to the boundary conditions

$$\left.\begin{aligned} &u_{s+1}(x, zN_z, t) = 0,\ N_{s+1}(x, zN_z, t) = 0,\ \theta_{s+1}(x, zN_z, t) = 1,\ \phi_{s+1}(x, zN_z, t) = 1 \\ &u_{s+1}(x, z_0, t) = 0,\ N_{s+1}(x, z_0, t) = 0,\ \theta_{s+1}(x, z_0, t) = 1,\ \phi_{s+1}(x, z_0, t) = 1 \end{aligned}\right\} \quad (41)$$

to yield the approximate numerical solution by writing a computer code using MATLAB.

3.1 Nusselt number, Sherwood number and Local Skin-friction Coefficient

The quantities of main engineering interest in the problem at hand are the Nusselt number, the Sherwood number, and the shearing stress on the plate. The Nusselt number and the Sherwood number physically indicate the rate of heat transfer and the rate of mass transfer respectively. The equation defining the wall shear stress is

$$\tau_w = (\mu + k)\left(\frac{\partial u}{\partial z}\right)_{z=0} + kN(z)_{z=0} \tag{42}$$

Thus, Skin Friction Coefficient, C_f, is computed as

$$C_f = \frac{2\tau}{\rho U_0^2} = \frac{2(\mu+k)}{\rho U_0^2}\left(\frac{\partial u}{\partial z}\right)_{z=0} = \frac{2}{U_0^2}[\nu + \Delta\nu]\left(\frac{\partial u}{\partial z}\right)_{z=0} = \frac{2}{U_0^2}[1+\Delta]\nu\left(\frac{\partial u}{\partial z}\right)_{z=0} \tag{43}$$

The above relation shows that the skin friction coefficient C_f is proportional to $\frac{1}{U_0^2}[1+\Delta]\nu\left(\frac{\partial u}{\partial z}\right)_{z=0}$. (44)

The Heat flux at the surface is calculated as

$$q_w = -\kappa\left(\frac{\partial T}{\partial z}\right)_{z=0} \tag{45}$$

The rate of heat transfer in terms of the Nusselt number at the plate is given by

$$Nu_x = \frac{-\kappa\left(\frac{\partial T}{\partial z}\right)_{z=0}}{(T_w - T_\infty)}\left(\frac{x}{\kappa}\right) = \frac{q_w}{(T_w - T_\infty)}\left(\frac{x}{\kappa}\right) \tag{46}$$

The mass flux is defined as follows

$$m_w = -D_M\left(\frac{\partial C}{\partial z}\right)_{z=0} \tag{47}$$

The rate of mass transfer in terms of the dimensionless Sherwood number is defined as follows

$$Sh_x = \frac{-xD_M\left(\frac{\partial C}{\partial z}\right)_{z=0}}{D_M(C_w - C_\infty)} = \frac{xm_w}{D_M(T_w - T_\infty)} \tag{48}$$

4 RESULTS AND DISCUSSION

The effect of various parameters on the Numerical solution of the Transient Free Convection in Magneto-Micropolar Fluid with Heat Generation, Mass Transfer and Constant Heat Flux has been investigated. Using the aforementioned numerical procedure, the numerical results obtained using the governing equations (36) -(39) subject to the boundary conditions (40) are displayed through graphs and tables below. To study the physical situation of these problems, we have computed the numerical values of the velocities, angular momentum, temperature, concentration, within the boundary layer and also found the skin friction coefficients, Nusselt and Sherwood number at the plate. It can be seen that the solutions are affected by the non-dimensional parameters and numbers, namely suction parameter S, local Grashof number Gr, local modified Grashof number Gc, permeability parameter K, Magnetic parameter M, Prandtl number Pr, Eckert number Ec, Dufour number Du, Schmidt number Sc, Soret number Sr, heat source parameter α, Micro inertia per unit mass J, Material parameter κ, Nusselt number Nu, Sherwood number Sh_x and dimensionless material (Micropolar) parameter Δ. The numerical solutions regarding the velocity, angular momentum, temperature and concentration distributions are presented for different selected values of the established dimensionless parameters. The influences of these various parameters on the velocity angular momentum, temperature and concentration fields are presented in Figure 2 through Figure 18 and some of the numerical results regarding coefficients skin friction and heat transfer are given in tabular form in Table 1 and Table 2. The results are discussed in section 4.2.

4.1 Results

4.1.1 Effect of various parameters on the velocity profiles

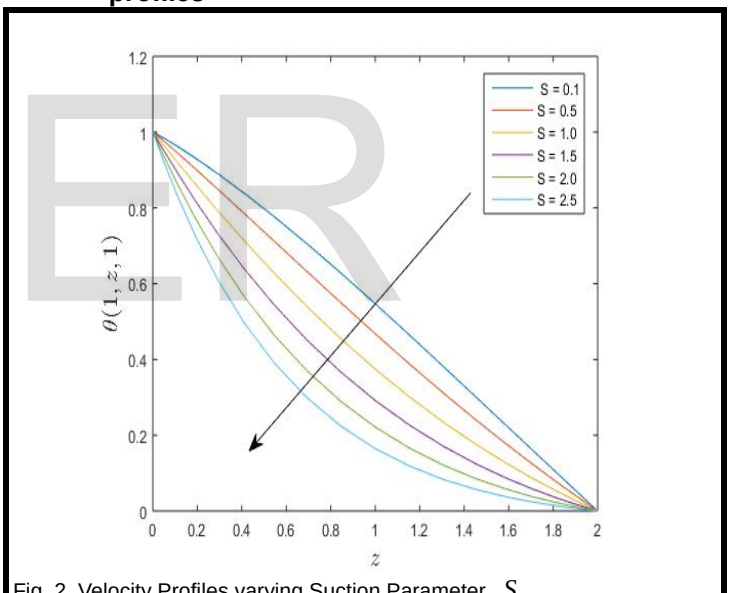

Fig. 2. Velocity Profiles varying Suction Parameter S

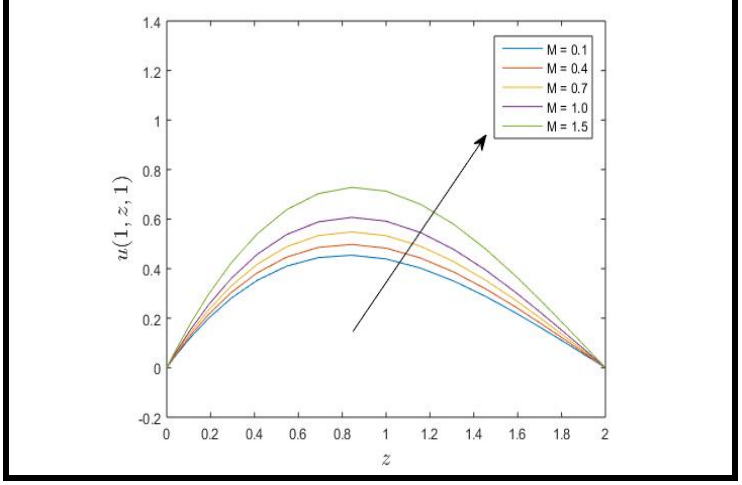

Figure 3: Velocity Profiles varying Magnetic Parameter M

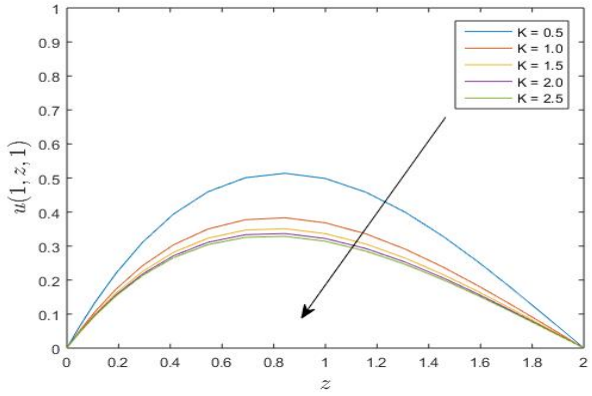

Fig. 4. Velocity Profiles varying Permeability Parameter K

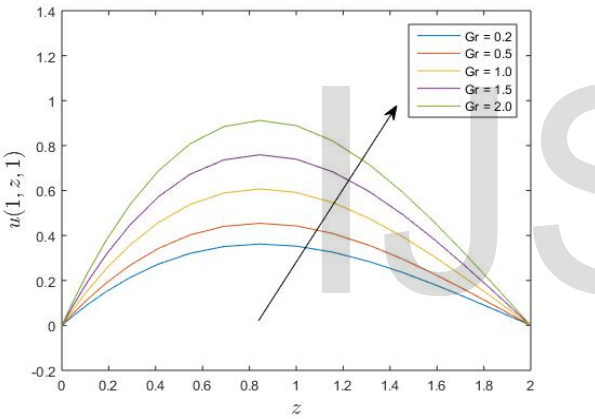

Fig. 5. Velocity Profiles varying Local Grashof Number Gr

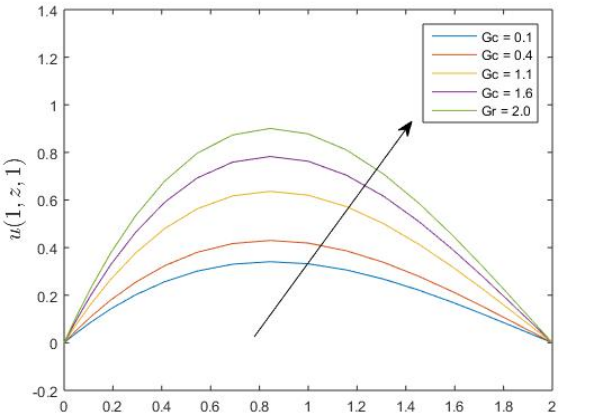

Fig. 6. Velocity Profiles varying Modified Grashof Number Gc

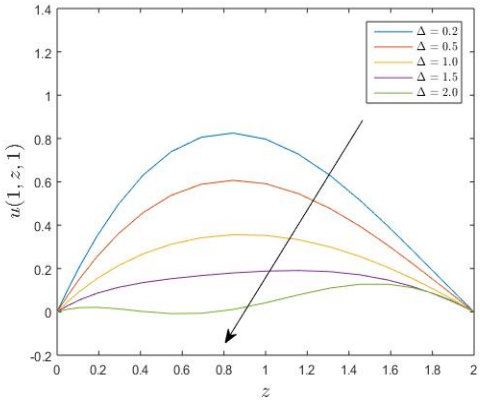

Fig. 7. Velocity Profiles varying Micro-rotation Parameter Δ

4.1.2 Angular Momentum Field Profiles

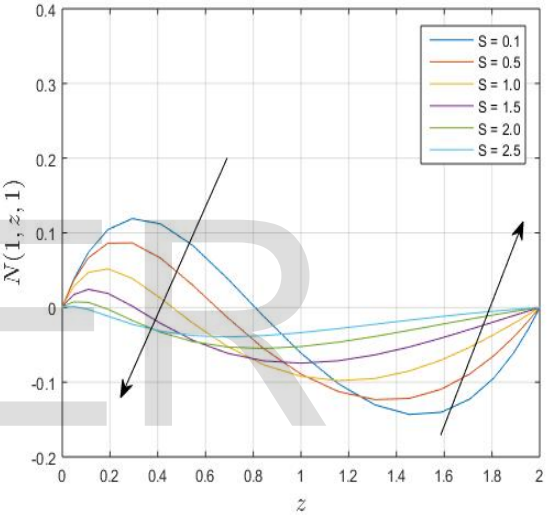

Fig. 8. Angular Momentum Field Profiles varying Suction Parameter S

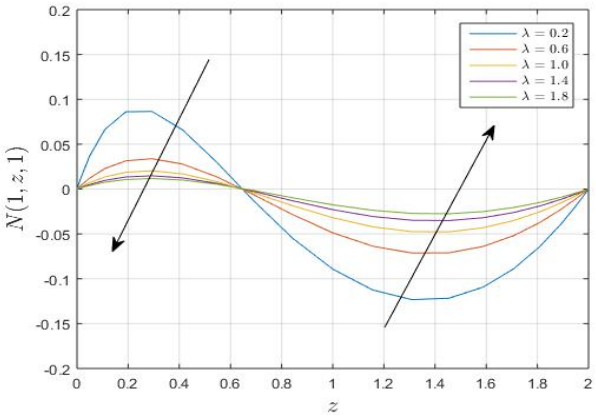

Fig. 9. Angular Mome ntum Field Profiles varying Dimensionless Material Parameter λ

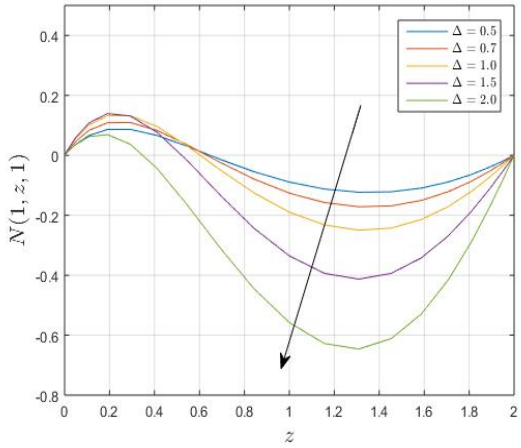

Fig. 10. Angular Momentum Field Profiles varying Micro-rotation Parameter Δ

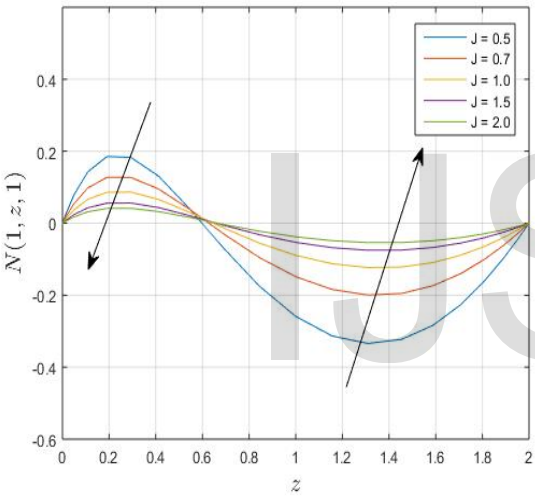

Fig. 11. Angular Momentum Field Profiles varying Micro inertia per unit mass J Parameter

4.1.3 Temperature Field Profiles

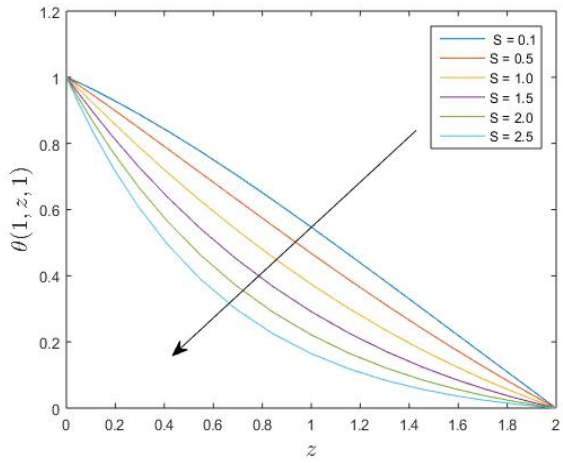

Fig. 12. Temperature Profiles varying Suction Parameter S

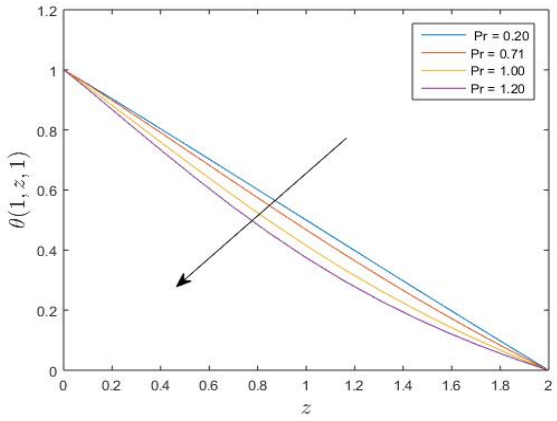

Fig. 13. Temperature Profiles varying Prandtl Number Pr

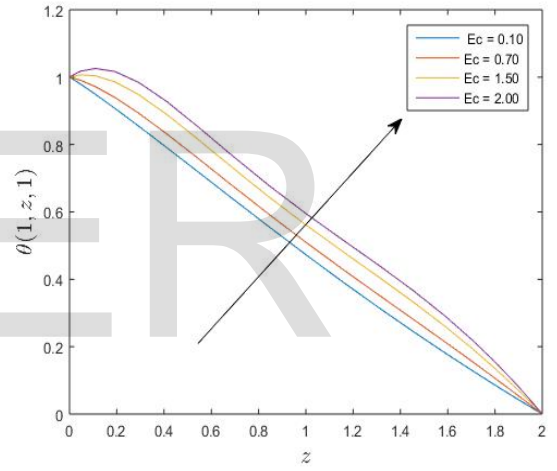

Fig. 14. Temperature Profiles varying Eckert Number Ec

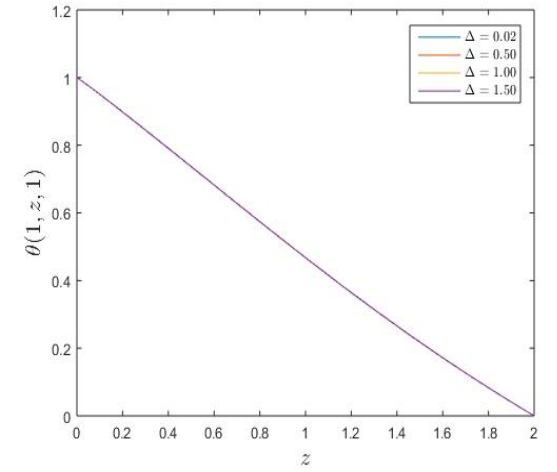

Fig. 15. Temperature Profiles varying Micro-rotation Parameter Δ

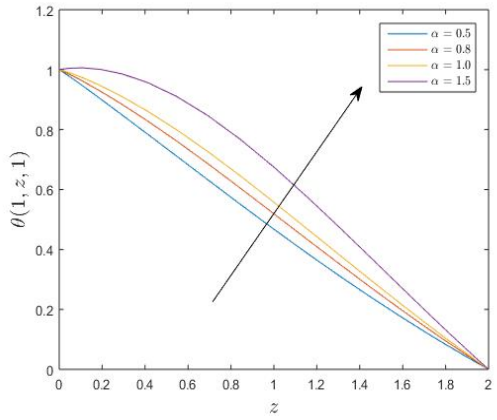

Fig. 16. Temperature Profiles varying Heat Source Parameter α

4.1.4 Concentration Field Profiles

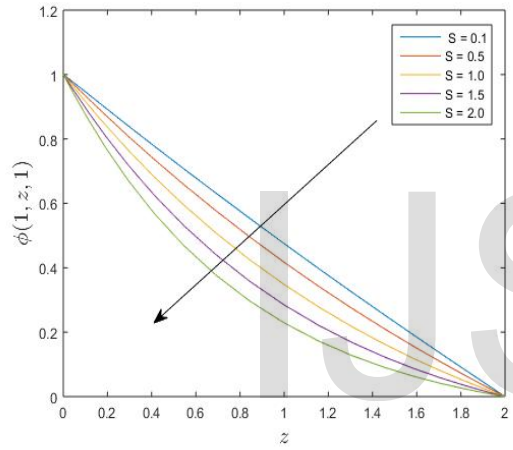

Fig. 17. Concentration Profiles varying Suction Parameter S

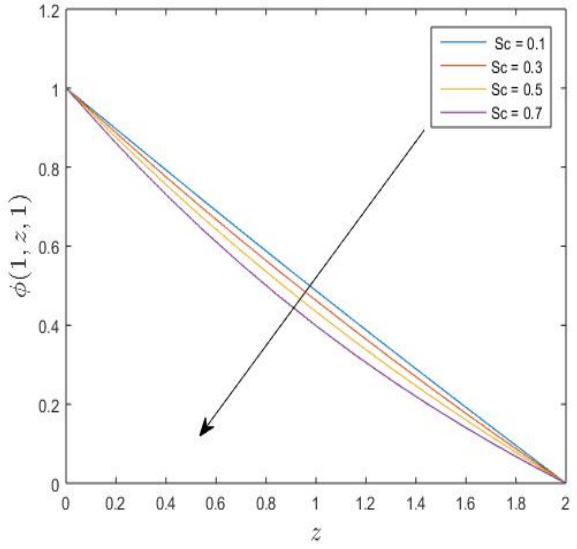

Fig. 18. Concentration Profiles varying Schmidt Number Sc

4.1.5 Computed values of skin friction, the local Nusselt number and Sherwood number

TABLE 1

VALUES OF Cf_x, Nu_x, Sh_x FOR DIFFERENT VALUES OF J

J	Present study			[21]	
	Cf_x	Nu_x	Sh_x	Cf_x	Nu_x
1.0	3.61662	-1.27121	-1.29801	3.27416	-1.18153
2.0	3.63745	-1.27089	-1.29801	3.26423	-1.18121
3.0	3.64335	-1.27078	-1.29801	3.26279	-1.18089
4.0	3.64613	-1.27073	-1.29801	3.26267	-1.18089
5.0	3.64775	-1.27070	-1.29801	3.26282	-1.18059
6.0	3.64881	-1.27067	-1.29801	3.26301	-1.18025

TABLE 2

VALUES OF Cf_x, Nu_x, Sh_x FOR DIFFERENT VALUES OF Δ

Δ	Present study			[21]	
	Cf_x	Nu_x	Sh_x	Cf_x	Nu_x
0.2	3.95161	-1.26175	-1.29766	3.51345	-1.14611
0.5	3.61682	-1.27057	-1.29766	3.27416	-1.18153
1.0	3.07482	-1.28045	-1.29766	3.02336	-1.23349
1.5	2.49479	-1.28614	-1.29766	2.86484	-1.28266
2.0	1.68753	-1.28960	-1.29766	2.75206	-1.33076
2.5	0.12885	-1.29321	-1.29766	2.66539	-1.37831

TABLE 3

VALUES OF Cf_x, Nu_x, Sh_x FOR DIFFERENT VALUES OF α

α	Present study			[21]	
	Cf_x	Nu_x	Sh_x	Cf_x	Nu_x
0.5	3.61682	-1.27057	-1.29766	3.27416	-1.18153
0.8	3.70005	-1.14084	-1.29766	6.20671	-3.68331
1.0	3.76059	-1.04774	-1.29766	8.55529	-6.38748
1.5	3.93275	-0.78698	-1.29766	15.51437	-17.49511
2.0	4.14135	-0.47553	-1.29766	23.76422	-35.84558
2.5	4.39726	-0.09525	-1.29766	33.10350	-62.54968

TABLE 4

VALUES OF Cf_x, Nu_x, Sh_x FOR DIFFERENT VALUES OF λ

λ	Present study			[21]	
	Cf_x	Nu_x	Sh_x	Cf_x	Nu_x
0.2	3.61682	-1.27057	-1.29766	3.27416	-1.18153
0.4	3.62175	-1.27051	-1.29766	3.24942	-1.18572
0.5	3.62388	-1.27048	-1.29766	3.24500	-1.18718
0.6	3.62584	-1.27045	-1.29766	3.24258	-1.18840
0.8	3.62931	-1.27039	-1.29766	3.24073	-1.19034
1.0	3.63223	-1.27035	-1.29766	3.24076	-1.19182

TABLE 5

VALUES OF Cf_x, Nu_x, Sh_x FOR DIFFERENT VALUES OF Pr

Pr	Present study			[21]	
	Cf_x	Nu_x	Sh_x	Cf_x	Nu_x
0.2	4.73292	-0.62824	-1.29766	7.927539	-2.109994
0.71	3.61682	-1.27057	-1.29766	9.822492	-4.726112
0.73	3.58278	-1.30321	-1.29766	9.869625	-4.819553
1.0	3.19873	-1.77259	-1.29766	10.446450	-6.076511

5.0	2.08072	-9.61183	-1.29766	16.005450	-27.739200
7.0	2.00606	-13.60821	-1.29766	18.124500	-40.557210

TABLE 6
VALUES OF Cf_x, Nu_x, Sh_x FOR DIFFERENT VALUES OF Gr

Gr	Present study			[21]	
	Cf_x	Nu_x	Sh_x	Cf_x	Nu_x
0.5	2.72811	-1.28170	-1.29766	9.822492	-4.726112
1.0	3.61682	-1.27057	-1.29766	11.018580	-2.537850
1.5	4.50914	-1.25664	-1.29766	12.156370	-1.796058
2.0	5.40612	-1.23971	-1.29766	13.238690	-1.416348 5
2.5	6.63904	-1.22026	-1.29766	14.273790	-1.182411 6
3.0	8.52117	-1.19810	-1.29766	15.268690	-1.022038

TABLE 7
VALUES OF Cf_x, Nu_x, Sh_x FOR DIFFERENT VALUES OF Sc

TABLE 8
VALUES OF Cf_x, Nu_x, Sh_x FOR DIFFERENT VALUES OF Ec

Ec	Present study			[19]	
	Cf_x	Nu_x	Sh_x	Cf_x	Nu_x
0.0	3.61091	-1.29678	-1.29766	1.44964	-0.226782
0.1	3.61682	-1.27057	-1.29766	1.60626	-0.247826
0.2	3.62275	-1.24415	-1.29766	1.86961	-0.232378
0.3	3.62870	-1.21753	-1.29766	2.35643	-0.216932
0.4	3.63468	-1.19071	-1.29766	2.61346	-0.188763
0.5	3.64068	-1.16368	-1.29766	2.83685	-0.167242

TABLE 9
VALUES OF Cf_x, Nu_x, Sh_x FOR DIFFERENT VALUES OF S

4.2 Discussion

Sc	Present study			[23]		
	Cf_x	Nu_x	Sh_x	Cf_x	Nu_x	Sh_x
0.1	4.86132	-1.24375	-0.59438	2.43066	-1.98056	-0.26445
0.2	4.57244	-1.25100	-0.70913	2.28622	-2.02576	-0.33746
0.3	4.29981	-1.25726	-0.83766	2.14991	-2.12458	-0.41345
0.4	4.04777	-1.26256	-0.97927	2.02389	-2.14224	-0.45176
0.5	3.81966	-1.26696	-1.13318	1.90983	-2.16882	-0.50124
0.6	3.61682	-1.27057	-1.29766	1.80841	-2.17432	-0.53824

From fig.3 Velocity u increases significantly on increasing the Magnetic parameter M. This is as a result of Lorentz force which acts in the direction of the fluid flow to produce drag thus creating resistance to the flow. This force increases the velocity of the fluid. Thus, we conclude that the magnetic field has accelerating influence on the fluid flow. Similarly, on varying magnetic parameter M and taking magnetic field to be a constant, the result agrees with L. Ramamohan Reddy *et al.*, (2017).

From fig. 8 increase in suction parameter S, angular momentum N decreases. This is owing to the fact that the suction decelerates the boundary layer flow. Greater suction corresponds physically to removal of micropolar fluid via the wall. This destroys momentum and causes the boundary layer to adhere to the wall thereby stabilizing boundary layer growth due to which the primary velocity of the fluid decreases. However, increasing the suction after the cross-over of the profiles, amounts to acceleration in velocity.

S	Present study			[22]		
	Cf_x	Nu_x	Sh_x	Cf_x	Nu_x	Sh_x
0.1	4.72706	-0.29448	-0.51702	1.7996514	-1.247951	-0.916867
0.5	4.62565	-0.45858	-0.65062	1.6512058	-1.263071	-0.930092
1.0	4.37718	-0.70206	-0.84229	1.4834408	-1.626014	-1.048395
1.5	4.02617	-0.98307	-1.05912	1.3037306	-1.800411	-1.106039
2.0	3.61150	-1.29417	-1.29766	1.1214543	-2.021411	-1.146248
2.5	3.17305	-1.62731	-1.55392	0.9470242	-2.248346	-1.175462

In Figure 12 Temperature θ monotonically decreases on increasing suction parameter S. This is attributed to the fact that thickness of the thermal boundary layer decreases with the increase of the suction parameter.

From Figure 13, Temperature θ monotonically decreases on increasing Prandtl number Pr. It is evident that the temperature in the boundary layer falls very quickly for large value of the Prandtl number because of the fact that thickness of the boundary layer decreases with decreases with an increase in the value of the Prandtl number.

From Figure 17, Concentration ϕ monotonically decreases on increasing Suction parameter S. The effect of increasing values of the suction parameter S is to decrease the Concentration boundary layer thickness which consequently decreases the concentration distribution.

From Figure 18, Concentration ϕ monotonically decreases on increasing Schmidt parameter Sc. The Schmidt number embodies the ratio of the momentum to the mass diffusivity. The Schmidt number therefore quantifies the relative effectiveness of momentum and mass transport by diffusion in the hydrodynamic (velocity) and concentration (species) boundary layers. It is observed that as the Schmidt number increases the concentration decreases.

In Tables 1-9, the numerical analysis of Cf_x, Nu_x and Sh_x on different physical parameters is displayed.

It is observed from tables 1, 3, 4, 6 and 8 that increase in Micro inertia per unit mass parameter J, Heat Source parameter α, Dimensionless material parameter λ, local Grashof number Gr and Eckert number Ec enhance the local skin-friction

coefficient Cf_x, but decreases local Nusselt number Nu_x while Sherwood number Sh_x remains constant. Increasing the value of Ec leads to an increase in the velocity of the fluid and hence the observed increase in the magnitude of the values of both shear stresses. Increasing Ec results to a lower rate of species transportation leading to a decrease in Sh_x. Increase in Ec translates to a lower value of the temperature difference, and to a reduced rate of heat transfer. Increase in α enhances convection currents on the surface of the sheet, leading to increase in Cf_x. Increase in α leads to a thicker thermal boundary layer, leading to lower temperature gradients leading to a decrease in Nu_x.

Moreover, from tables 2, 5, 7, and 9, the local Skin friction falls by enlarging the viscosity ratio (Micropolar parameter) Δ, Prandtl number $\Pr$, Schmidt number Sc and Suction parameter S but enhances the local Nusselt number Nu_x while Sherwood number Sh_x remains constant for Δ and $\Pr$. Increase in Sc and S enhances the Sherwood number Sh_x. Increase in Δ leads to a thinner thermal boundary layer, resulting to an increased rate of heat transfer. Decrease in the velocity profiles leads to a reduced rate of transportation of species away from the surface of the stretching sheet, leading to the observed increase in the value of Sh_x. Suction accelerates the velocity of the fluid particles leading to higher flow velocities. Thermal boundary layer thickness decreases with increase in S, leading to an increased rate of heat transfer. Decrease in concentration boundary layer thickness leads to an increased rate of species transportation, and hence to increase in the Sherwood number Sh_x.

From the table 1 it is observed that the coefficient proportional to the skin friction increases primarily (from 1 to 4) then decreases. In both cases the rate of change is very small. Whereas in the case of Nusselt number the rate of decrease is monotonous, although slow. Thus, it may be considered that the micro inertia has a very little impact on the coefficient of skin friction and Nusselt numbers.

In the table 2 only the dimensionless material parameter λ has been varying, keeping other parameters as fixed. It is observed that both the tabulated values are decreasing with the increase in Δ and the rate of decrease has no significant difference. It can be observed that there is an inverse behavior of the curves. This can be explained from the fact that viscosity is taken to vary inversely proportional to temperature thus a varying change of the curves.

5 Conclusion

i. Skin friction Cf_x increases with increasing J, α, λ, Gr, Ec and Nu_x decreases with increasing Δ, $\Pr$, Sc and S

ii. Nusselt number Nu_x increases with increasing Δ, $\Pr$, Sc, S while Nu_x decreases with increasing J, α, λ, Gr, and Ec.

iii. Sherwood number Sh_x increases with enhancing Sc, S but remains constant on increasing the parameters J, Δ, α, λ, $\Pr$, Gr, and Ec.

iv. The velocity profiles are enhanced on increasing M, Gr, Gc and falls on increasing S, K, Δ. Magnetic field has accelerating influence on the fluid flow, as a result of Lorentz force which acts in the direction of the fluid flow. On increasing suction parameter S, velocity u increases in the case of injection. This is due to increase in pressure forces which causes the fluid to accelerate.

v. The angular momentum profiles increase with increasing S, λ, J. However, they decrease in the reverse direction on increasing Δ, λ, S, J. This behaviour is accounted for by that fact this layer presents a transition state after which the opposite effect, i.e. $|h(\eta)|$ increases with an increasing λ till the free stream state is attained.

vi. Increasing the parameters Ec and α increases the temperature profiles but decreases on increasing S and $\Pr$ while the temperature profiles are not affected on increasing Δ.

vii. Concentration profiles decreases on increasing S and Sc.

Acknowledgment

The authors wish to thank National Commision for Science, Technology and Innovation. This work was supported in part by a grant from National Commision for Science, Technology and Innovation.

References

[1] Hosain, M. L., Fdhila, R. B., & Daneryd, A. (2016). Heat transfer by liquid jets impinging on a hot flat surface. *Applied energy*, 164, 934-943.

[2] Sharma, C. S., Tiwari, M. K., Zimmermann, S., Brunschwiler, T., Schlottig, G., Michel, B., & Poulikakos, D. (2015). Energy efficient hotspot-targeted embedded liquid cooling of electronics. *Applied Energy*, 138, 414-422.

[3] Park, J. U., Hardy, M., Kang, S. J., Barton, K., Adair, K., Kishore Mukhopadhyay, D., ... & Ferreira, P. M. (2007). High-resolution electrohydrodynamic jet printing. *Nature materials*, 6(10), 782.

[4] Arias, A. C., Ready, S. E., Lujan, R., Wong, W. S., Paul, K. E., Salleo, A., ... & Liu, P. (2004). All jet-printed polymer thin-film transistor active-matrix backplanes. *Applied Physics Letters*, 85(15), 3304-3306.

[5] Lin, L., Peng, H., & Ding, G. (2016). Influence of oil concentration on wetting behaviour during evaporation of refrigerant–oil mixture on copper surface. *International Journal of Refrigeration*, 61, 23-36.

[6] Badr, S., Gauthier, G., & Gondret, P. (2014). Erosion threshold of a liquid immersed granular bed by an impinging plane liquid jet. *Physics of Fluids*, 26(2), 023302.

[7] Misra, J. C., & Ghosh, S. K. (2001). A mathematical model for the

study of interstitial fluid movement vis-a-vis the non-Newtonian behaviour of blood in a constricted artery. *Computers & Mathematics with Applications*, 41(5-6), 783-811.

[8] Papautsky, I., Brazzle, J., Ameel, T., & Frazier, A. B. (1999). Laminar fluid behaviour in microchannels using micropolar fluid theory. *Sensors and actuators A: Physical*, 73(1-2), 101-108.

[9] Harrison, D. J., Manz, A., & Glavina, P. G. (1991, June). Electroosmotic pumping within a chemical sensor system integrated on silicon. In *Proc. of Int. Conf. on Solid-State Sensors and Actuators Transducers*, 792-795.

[10] Giamberini, M., Amendola, E., & Carfagna, C. (1997). Lightly cross-linked liquid crystalline epoxy resins: The effect of rigid-rod length and applied stress on the state of order of the cured thermoset. *Macromolecular Chemistry and Physics*, 198(10), 3185-3196.

[11] Borgohain, B. (2015). Micropolar fluid over a stretching surface in a non-Darcian porous medium when viscosity and thermal conductivity vary with temperature in presence of magnetic field, *International Research Journal of Mathematics, Engineering and IT*, 2(10), ISSN: (2349-0322)

[12] Eringen, A. C. (1972). Theory of thermomicrofluids. *Journal of Mathematical Analysis and Applications*, 38(2), 480-496.

[13] Lukaszewicz, G. (1999). *Micropolar fluids: theory and applications*. Springer Science & Business Media.

[14] Koriko, O. K., Omowaye, A. J., Animasaun, I. L., & Bamisaye, M. E. (2017). Melting heat transfer and induced-magnetic field effects on the micropolar fluid flow towards stagnation point: Boundary layer analysis. In *International Journal of Engineering Research in Africa*, 29, 10-20. Trans Tech Publications.

[15] S. Madhavi Latha, D.R.V. Prasada Rao (2017), Finite element analysis of convective heat and mass transfer flow past a vertical porous plate in a rotating fluid with chemical reaction, dissipation, Soret and Dufour effects, *International Journal of Emerging Trends in Engineering and Development*, 3(7), ISSN 2249-6149

[16] Maraka, W. M., Ngugi, K. M., & Roy, K. P. (2018). Similarity Solution of Unsteady Boundary Layer Flow of Nanofluids past a Vertical Plate with Convective Heating. *Global Journal of Pure and Applied Mathematics*, 14(4), 517-534.

[17] Baruah, I., & Hazarika, G. C. (2017). Effects of Variable Viscosity and Thermal Conductivity of Unsteady Micropolar Fluid under Mixed Convection in Presence of Uniform Magnetic Field on Stretching Surface. *International Journal of Computer Applications*, 166(3).

[18] Govardhan, K., Nagaraju, G., Kaladhar, K., & Balasiddulu, M. (2015). MHD and radiation effects on mixed convection unsteady flow of micropolar fluid over a stretching sheet. *Procedia Computer Science*, 57, 65-76.

[19] Atif, S. M., Hussain, S., & Sagheer, M. (2018). Numerical study of MHD micropolar carreau nanofluid in the presence of induced magnetic field. *AIP Advances*, 8(3), 035219.

[20] Mohammad, A., & Mohammad, S. A. (2013). Soret and Dufour Effects on Steady Free Convective in MHD Micropolar Fluid Flow, Mass and Heat Transfer with Hall Current. *International Journal of Advancements in Research and Technology*, 2, 130-138.

[21] Rashid, G. M. (2012). Transient Free Convection in Micropolar Fluid with Heat Generation and Constant Heat Flux (Doctoral dissertation, Khulna University of Engineering & Technology (KUET), Khulna, Bangladesh.).

[22] Haque, M. Z., Alam, M. M., Ferdows, M., & Postelnicu, A. (2012). Micropolar fluid behaviours on steady MHD free convection and mass transfer flow with constant heat and mass fluxes, joule heating and viscous dissipation. *Journal of King Saud University-Engineering Sciences*, 24(2), 71-84.

[23] Uwanta, I. J., & Usman, H. (2014). On the Influence of Soret and Dufour Effects on MHD Free Convective Heat and Mass Transfer Flow over a Vertical Channel with Constant Suction and Viscous Dissipation. *International scholarly research notices*.

[24] Turk, M. A., Sylvester, N. D., & Ariman, T. (1973). On pulsatile blood flow. *Transactions of the Society of Rheology*, **17**(1), 1-21.

[25] Eijkel, J. C., & van den Berg, A. (2006). The promise of nanotechnology for separation devices–from a top-down approach to nature-inspired separation devices. *Electrophoresis*, **27**(3), 677-685.

[26] Reddy, L. R., Raju, M. C., Raju, G. S. S., & Ibrahim, S. M. (2017). Chemical reaction and thermal radiation effects on MHD micropolar fluid past a stretching sheet embedded in a non-Darcian porous medium. *Journal of Computational and Applied Research in Mechanical Engineering*, *6*(2), 27-46.